Indonesian Journal of Environmental Management and Sustainability
e-ISSN:2598-6279 *p*-ISSN:2598-6260

IJEMS

Research Paper

Acid-Activated Natural Clay for Fe(III) Adsorption: An Integrated Study of Mechanisms, Kinetics, and Thermodynamics

Moh. Azhar Afandy[1*], Deden Jajang Harly Herliawan[1], Nirwansyah[1], Fikrah Dian Indrawati Sawali[1]

[1] *Mineral Chemical Engineering, Politeknik Industri Logam Morowali, Morowali, Central Sulawesi, 94974, Indonesia*
***Corresponding author e-mail**: azhar@pilm.ac.id

Abstract
The increasing contamination of water by Fe(III) ions from industrial activities, particularly in nickel-producing regions such as Morowali, presents serious environmental and public health concerns. Among various treatment approaches, adsorption stands out as an efficient and cost-effective method, especially using natural clay modified by acid treatment. This study aims to investigate the characterization, adsorption kinetics, and thermodynamic behavior of Fe(III) removal using acid-modified natural clay (NC) derived from Morowali. The clay was activated using sulfuric acid (H_2SO_4), followed by physicochemical characterization and batch adsorption experiments to assess its removal performance. Adsorption kinetics were analyzed using Pseudo-First Order (PFO), Pseudo-Second Order (PSO), Intraparticle Diffusion (IPD), and Liquid Film Diffusion (LFD) models to elucidate the adsorption mechanism. Furthermore, thermodynamic parameters such as Gibbs free energy (ΔG°), enthalpy (ΔH°), and entropy (ΔS°) were calculated to determine the nature of the adsorption process. The results showed that NC exhibited a considerable adsorption capacity for Fe(III), with PSO providing the best kinetic fit, indicating chemisorption control. Thermodynamic analysis confirmed the spontaneous and endothermic nature of the process. These findings demonstrate the potential of acid-modified clay from Morowali as a low-cost and locally available adsorbent, contributing to sustainable water treatment strategies in industrial regions.

Keywords
Adsorption, Fe(III), Natural Clay, Kinetics, Thermodynamics

Received: 20 April 2025, Accepted: 7 July 2025
https://doi.org/10.26554/ijems.2025.9.3.143-155

1. INTRODUCTION

Fe(III) ion is a form of heavy metal that typically pollutes places with highly developed industrial operations, particularly advancements in the nickel industry. Fe(III) waste is generally found in acid mine water and contaminated groundwater, and will subsequently affect the surrounding environment and ecology if not immediately handled (Abdel-Ghafar et al., 2020; Ngkoimani and Chaerul, 2017). The existence of Fe(III) in water can cause challenges, particularly, the water becomes unclear has an unappealing smell and color in drinking water, also can enhance the production of iron sediment, which may affect aquatic ecosystems (Das and Nandi, 2019; Islam and Mostafa, 2024). Drinking freshwater containing Fe(III) can cause health problems such as heavy metal poisoning, digestive system illnesses, and even death and can degrade the quality of health of individuals who reside around industrial sites (Abbaspour et al., 2014; Latunde-Dada, 2024). Therefore, an effective, efficient, and economical solution is needed to eliminate or minimize Fe(III) contaminants produced by industrial activities.

Many different types of techniques have been employed in attempting to minimize Fe(III) contamination such as chemical precipitation, ion flotation, membrane filtration, electrochemical treatment, chlorine dioxide, coagulation, aeration and adsorption (Islam and Mostafa, 2024; Khatri et al., 2017; Kulkarni, 2016; Oladimeji et al., 2024; Purnamasari and Supraptiah, 2017; Thinojah and Ketheesan, 2022). From all of these techniques, adsorption is one of the most used methods since it has the advantage of relatively low costs, high efficiency, and the capacity to remove contaminants in low concentrations (Enaime et al., 2020; Nahiun et al., 2021; Pakade et al., 2019; Raji et al., 2023; Wang et al., 2023). The application of the adsorption method also makes it feasible to utilize organic materials and waste as adsorbents such as coffe waste (Zein et al., 2023), fruit peel derived-biochar (Adawiyah et al., 2021), Rice Husk (Herrera et al., 2022; Kumar et al., 2023; Li et al., 2023; Palapa et al., 2023), consequently providing an additional benefit to environmental sustainability.

Natural clay is a mineral with significant benefits as an adsorbent (Bahabadi et al., 2016; Middea et al., 2024. In the nickel industrial area, such as Indonesia, specifically in the Morowali area, the demand for inexpensive and effective waste processing technology is quite important. The substantial abundance of natural clay in this area can be a sustainable local solution to overcome Fe(III) pollution. Several earlier investigations have identified the capabilities of natural clay in an effort to minimize heavy metal contamination. Research conducted by Wang et al. (2024), demonstrates that clay minerals for example kaolinite, montmorillonite, and bentonite offer huge potential for removing heavy metals from soil and water sources due to their inherent availability, low expense, and high efficacy. Other research performed by Xie et al. (2024), suggests that the utilization of natural clay minerals has very broad potential in the application of adsorption technology in an effort to reduce heavy metal pollution. Based on this, this research was undertaken by leveraging the potential of natural clay, specifically in the Morowali area, which can be used as raw material for adsorbents and can also give local and sustainable solutions to tackle Fe(III) contamination in the area.

To enhance the adsorption capacity of natural clay, modification is performed with sulfuric acid to further enhance its chemical and physical characteristics. This procedure entails the extraction of soluble cations and the expansion of clay layers, consequently augmenting the specific surface area and the quantity of active sites on the material's surface (Osmić et al., 2024). Moreover, acid modification can alter the crystal structure of clay to become more amorphous, hence enhancing its affinity for metal ions such as Fe(III) (Rosa et al., 2020; Song et al., 2023). The modified natural clay, including a higher concentration of dominant acid functional groups on its surface, facilitates increased electrostatic interactions and complexation with heavy metals.

Many earlier studies have centered on the efficiency of Fe(III) removal, neglecting a comprehensive review of material properties, adsorption methods, and kinetic and thermodynamic aspects. The Morowali region contains an abundance of natural clay, which holds significant potential as a local resource for industrial waste disposal. However, research specifically employing Morowali clay as an adsorbent for Fe(III) waste treatment remains limited. This is an opportunity to investigate the advantages of local materials in delivering sustainable and cost-effective solutions. The current research aimed to examine both the chemical and physical attributes of clay modified with sulfuric acid (H_2SO_4), evaluate the kinetic mechanisms of the Fe(III) adsorption process via different models involving pseudo first order, pseudo second-order intra-particle diffusion, and liquid film diffusion, as well as thermodynamic factors such as Gibbs free energy (ΔG°), enthalpy (ΔH°), and entropy (ΔS°) in order to clarify the spontaneity and energy characteristics associated with the Fe(III) adsorption phase. This study desires to provide a thorough theoretical basis for the characterization, kinetic mechanisms, and thermodynamics of Fe(III) adsorption utilizing modified natural clay, while also providing an economical and environmentally friendly practices wastewater treatment technology for industrial applications.

2. EXPERIMENTAL SECTION

2.1 Materials

The materials utilized in the current study are natural clay, sulfuric acid 98% (H_2SO_4), hydrochloric acid 37% (HCl), iron (III) chloride hexahydrate ($FeCl_3.6H_2O$), potassium permanganate ($KMnO_4$), oxalic acid ($H_2C_2O_4$), ferrous aluminum sulfate (FAS), distilled water, and potassium thiocyanate (KSCN). All chemicals utilized in the current study originated from local suppliers with Merck, Germany specifications.

2.2 Adsorbent Preparation

Natural clay (NC) utilized in this study was acquired from the Witaponda area, Morowali, with a high waters content. The water removal approach was first carried out by drying under sunlight for ± 7 days. Furthermore, the drying procedure was carried out by putting NC into an oven at a temperature of 110°C for ± 12 hours. After that, a size reduction technique was carried out using a mortar to a size of 60 mesh. Then the activation process was carried out using 2 M H_2SO_4 (300 g NC in 1 L of H_2SO_4) similar to the procedure by Auta and Hameed (2013) with a few modifications. The activation procedure was carried out by stirring on a hot plate and magnetic stirrer at a temperature of 90°C for ± 4 hours. The activated NC adsorbent was then filtered and washed to eliminate impurities using distilled water to a pH of 6.8-7. Furthermore, the calcination procedure was carried out using a furnace at a temperature of 550°C for 4 hours. The obtained NC adsorbent is ready to be applied as illustrated in Figure 1.

2.3 Characterization of NC

The surface morphology of the NC adsorbent was analyzed utilizing a scanning electron microscope (SEM) (JEOL JCM 6000plus), The functional groups examination of the samples was undertaken with Fourier Transform Infrared Spectroscopy (FTIR) (Shimadzu IRP Prestige'21) across the frequency range between 4000-400 cm^{-1}.

2.4 Batch Adsorption Process

The method for the adsorption procedures was conducted in in batches by using a 250 mL Erlenmeyer flask that includes 100 mL of a solution consisting of Fe(III) with several lengths of time (30-180 minutes). The solution containing Fe(III) has been generated by dissolve a specific quantity of $FeCl_3.6H_2O$ with distilled water. The NC adsorbent was then added with a variation of NC mass (0.5-1 g) to see the influence of NC mass on the adsorption process and was

Table 1. Kinetic Models

Kinetic Models	Equation	References
Pseudo-First-Order (PFO)	$\log(q_e - q_t) = \log q_e - \frac{k_1}{2.303}t$ (2)	(Benjelloun et al., 2021)
Pseudo-Second-Order (PSO)	$\frac{t}{q_t} = \frac{1}{k_2 q_e^2} + \frac{t}{q_e}$ (3)	(Šuránek et al., 2023)
Fractional Power (FP)	$\ln q_t = \ln a + b \ln t$ (4)	(Salam et al., 2014)
Intraparticle Diffusion (IPD)	$q_t = K_{\text{int}}\, t^{1/2} + C$ (5)	(Menkiti et al., 2018)
Bangham	$\log\log\left(\frac{c_0}{c_0 - mq_t}\right) = \log\left(\frac{K_B m}{2.303V}\right) + \alpha \log t$ (6)	(Inyinbor et al., 2016)
Liquid-film diffusion (LFD)	$\ln\left(1 - \frac{q_t}{q_e}\right) = -Kt$ (7)	(Al-Odayni et al., 2023)

performed at a temperature of ± 28°C for 12 hours. The final concentration of Fe(III) has been determined using a visible spectrophotometer (ICEN IN-B046) in a wavelength of 510 nm similar to the approach carried out by Sirotiak et al. (2014). The amount of Fe(III) adsorbed by the NC adsorbent could be calculated via Equation 1.

$$q_t = \frac{(C_o - C_t) \times V}{m} \quad (1)$$

The qt value represents the adsorption capacity measured in mg.g^{-1}. Co refers to the initial concentration of Fe(III) (mg.L^{-1}). Ct demonstrates the concentration of Fe(III) at time t, also in mg L^{-1}. V refers to the volume of Fe(III) (L), while m signifies the mass of the adsorbent (g).

2.5 Kinetics Study

Several Kinetics model equations used to evaluate the kinetic parameters that occur in the adsorption process can be seen in Table 1.

Where R is the ideal gas constant (J.mol^{-1}.K^{-1}), T is temperature (K), Kc is the adsorption equilibrium constant, k_1 is the first-order rate constant (min^{-1}), k_2 is the second-order rate constant (g.mg^{-1}.min^{-1}), a is the constant for fractional power kinetics (mg.g^{-1}.min^{b}), and b is the fractional power exponent. K_{int} is the intraparticle diffusion rate constant (mg.g^{-1} min$^{-1/2}$), C is the boundary layer thickness (mg.g^{-1}), α is the Bangham exponent parameter, K_B is the Bangham diffusion rate constant (g), K_{fd} is the liquid film diffusion rate constant (min^{-1}), and $t_{1/2}$ is the half-lifetime (min).

2.6 Thermodynamics Study

Thermodynamic investigations have been performed to examine the mechanism and basic parameters of the interaction between NC adsorbent and Fe(III) as adsorbate. The equations utilized for thermodynamic studies are as follows (Guo et al., 2020; Yang et al., 2020):

$$\Delta G^\circ = -RT \ln K_C \quad (8)$$

$$\Delta G^\circ = \Delta H^\circ - T\Delta S^\circ \quad (9)$$

$$\ln K_C = \frac{\Delta S^\circ}{R} - \frac{\Delta H^\circ}{RT} \quad (10)$$

ΔH° represents the enthalpy (kJ/mol·K), ΔS° denotes the entropy (kJ/mol·K), and ΔG° signifies the Gibbs free energy (kJ/mol).

3. RESULT AND DISCUSSION

3.1 Characterization of NC Adsorbent

3.1.1 SEM Analysis

After the activation procedure by H_2SO_4, it shows some changes on the surface of the NC adsorbent as illustrated in

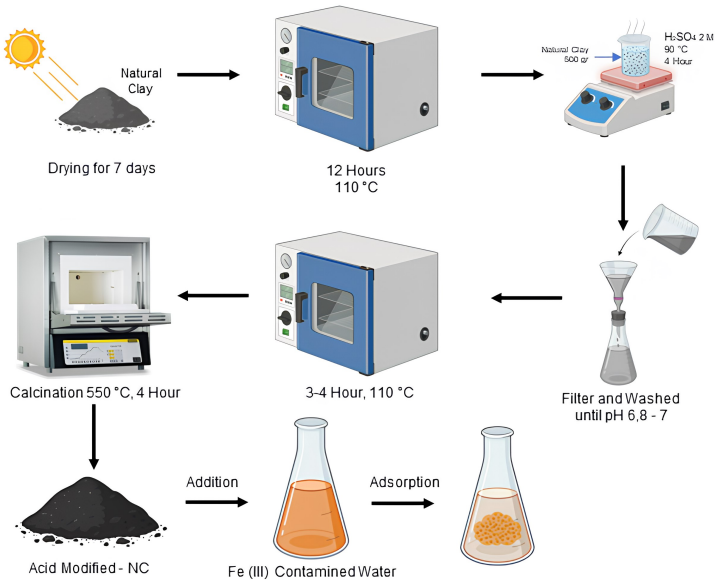

Figure 1. Procedure for Acid-Modified NC Preparation and Its Application for Fe(III) Removal

Table 2. Adsorption Capacity of Different Adsorbents for Fe(III) Removal

Adsorbent	qe (mg.g^{-1})	References
Acid-modified Natural Clay	18.36	This work
Chitosan flakes	82.30	(Costea et al., 2024)
Peganum harmala L. Plant	65.00	(Alsaiari et al., 2024)
Rice husk-activated carbon	28.90	(Elewa et al., 2023)
Perlite	4.45	(Kalabegashvili et al., 2022)
Palmyra palm fruit fibers biosorbent	0.41	(Satchawan et al., 2022)
Fluorapatite Extracted from Natural Phosphate	26.18	(Billah et al., 2021)
Zeolite	10.19	(Bakalár et al., 2020)
Bentonite	16.65	(Bakalár et al., 2020)
Transition metal oxide nanocomposite	22.03	(Langeroodi et al., 2018)
Tamarind Seeds	0.019	(Mopoung et al., 2015)

Figure 2. Activation with H_2SO_4 can produce attrition on the NC surface due to the removal of the ions including Al, Fe, and Mg, resulting in a surface that tends to be rougher and unequal. The decision to use of an acid activator depends on its capacity to eliminate contaminants, including metal oxides and exchangeable cations, while enhancing porosity and the quantity of active sites by leaching structural ions like Al^{3+} and Fe^{3+}. Moreover, acid activation can markedly enhance the surface area and pore volume, hence improving adsorption efficacy, rendering it a more advantageous option for heavy metal adsorption than base activation. The structure on the surface that was soon after solid will appear more porous and endure fragmentation owing to acid damage. The formation of holes or pores on the NC surface can be generated due to the dissolution of minerals in the NC during the activation process, which will subsequently increase the specific surface area and affect the adsorption capacity of the NC.

The adsorption of Fe(III) ions by NC results in surface alterations that reflect interactions between Fe(III) as the adsorbate and NC as the adsorbent. Figure 3 illustrates the presence of Fe(III) on the NC surface, evidenced by the formation of a thin layer or microscopic particles. These appear as brighter regions in the SEM image due to Fe(III), a heavier element, producing a more intense secondary electron signal. Fe(III) exhibits more electron density than NC minerals, resulting in a region of enhanced contrast in the SEM picture relative to the NC constituent elements (Al, Si, or O). A high number of Fe(III) on the adsorbent surface is evidenced by a rougher surface structure compared to its state prior to adsorption, attributed to metal deposits that alter the surface morphology of the NC adsorbent. The

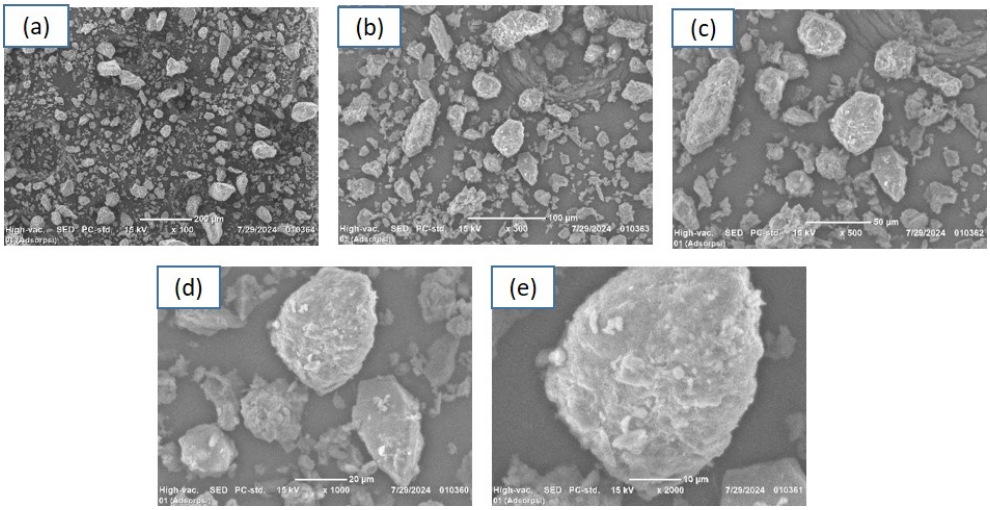

Figure 2. SEM Micrograph Before Adsorption: (a) 100×; (b) 300×; (c) 500×; (d) 1000×; (e) 2000×

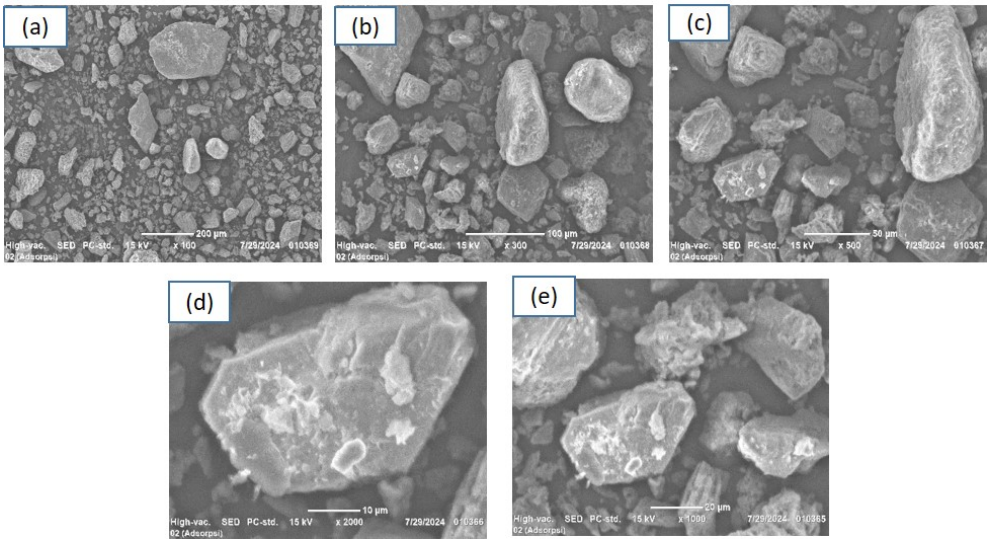

Figure 3. SEM Micrograph After Adsorption: (a) 100×; (b) 300×; (c) 500×; (d) 1000×; (e) 2000×

interaction between NC and Fe(III) further promotes the formation of larger agglomerates, as NC particles connect through ionic bridges formed by Fe(III), as shown in Figure 3. The presence of Fe(III) on the adsorbent surface can also block existing pores, thereby reducing the porosity of NC, as illustrated in Figure 3.

3.1.2 FTIR Analysis

The FTIR spectrum of NC may clarify the functional groups present in the substance. NC comprises many minerals, such as kaolinite, montmorillonite, and illite, each exhibiting a distinct infrared spectrum. The findings of the FTIR study are illustrated in Figure 4. The unactivated NC sample exhibits stretching vibrations of the group of hydroxyl (−OH) within the range of 3000-3800 cm^{-1}. The pronounced peaks resulting from water adsorption on the NC surface and water confined between mineral layers, attributable to hydrogen interactions among water molecules, signify the porosity of NC, which possesses the ability to absorb and retain substantial quantities of water. The peak at around 3620-3700 cm^{-1} signifies the presence of a −OH group associated with Al. The elevated water content signifies that the mineral present in NC is Montmorillonite, which possesses a greater interlayer water content than other minerals like kaolinite and illite (Caccamo et al., 2020). A peak in the range of 500–600 cm^{-1} indicates Al−O vibrations, while the peak near 780 cm^{-1} is attributed to symmetric bending of silica (Si−O−Si) or aluminate (Al−O−Al) groups, as well as quartz, which typically exhibits absorption near 775–800 cm^{-1}. The band at approximately 1600 cm^{-1} arises from the deformation of adsorbed water molecules within the NC structure, consistent with its high water absorption capability. During the

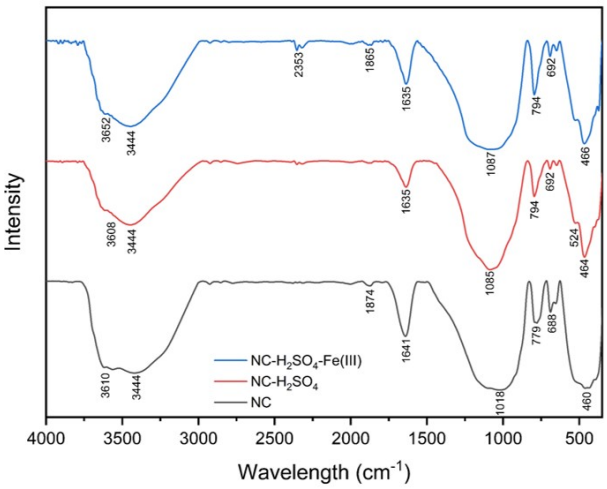

Figure 4. FTIR Spectra of NC, NC-H_2SO_4, and NC-H_2SO_4-Fe(III)

H_2SO_4 activation stage on NC, there were many changes in the IR spectra, such as a decrease in the strength of the hydroxyl group peak (−OH) at 3600-3700 cm^{-1}, which could occur due to the releasing of the Al−O bond caused by acid assault. In addition, there was a drop in intensity in the range of 1630-1650 cm^{-1} produced by the reduction of water molecules adsorbed or bound to NC due to the action of acid. The sharper peak around 1000-1100 cm^{-1} was due to acid activation, which induced the enrichment of silanol groups (−Si−OH) due to the loss of the alumina layer from the NC structure. Acid activation may affect the tetrahedral structure of the silicate, resulting in a peak shift (Si−O−Si). A reduction in intensity was also observed in the 1600-1700 cm^{-1} region, likely due to water desorption or changes in water interactions with the NC surface caused by acid-induced structural alterations. Additionally, a decrease in intensity within 600–750 cm^{-1} suggests that H_2SO_4 activation affected the crystalline structure of clay minerals, such as montmorillonite or kaolinite, potentially modifying the silicate framework and weakening the Si−O−Si bonds.

Following the adsorption process of Fe(III) by NC that has been activated by H_2SO_4 shows a few changes in the intensity at 3000-3800 cm^{-1}, where there is an increase again in the hydroxyl group (−OH) caused by the formation of hydrogen bonds generated between the Fe(III) and the hydroxyl group that exists on the NC surfaces. The higher intensity at 750-800 cm^{-1} thus reveals the relationship between metal bonds with oxygen (Fe−O) or (Fe−OH) if there are water molecules present such that it narrows the peak associated with metal-oxygen vibrations and shows a fairly solid and specific bond between Fe−O or Fe−OH. In addition, the interaction between Fe(III) and the silicate group can generate a Fe(III)-silicate complex that can alter the intensity at 750-800 cm^{-1}. This sharp rise may potentially be attributed to the increase in covalent connections between Fe(III) and oxygen in NC. If there is re-crystallization or a decrease in sulfuric acid strength, Fe(III) ions might bind more strongly to the NC surface, resulting in a sharper or higher peak around 700–800 cm^{-1}. The weak peak intensity at 2250–2300 cm^{-1} may be induced by the interaction of CO_2 or other functional groups with Fe(III) ions adsorbed on the NC surface. Fe(III) ions reacting with carboxylate groups or CO_2 groups can produce faint peaks in this region. Weak intensity is also exhibited in the band above 3700 cm^{-1}. The weak peak at 3700 cm^{-1} may suggest the presence of hydroxyl (OH) groups adsorbed on the NC surface after activation with H_2SO_4. Activation with acid can modify the surface structure of NC and improve the solubility of some components, allowing additional OH groups to be adsorbed. Fe(III) ions adsorbed on the NC surface can interact with these OH groups, reflecting the peak or modifying its shape.

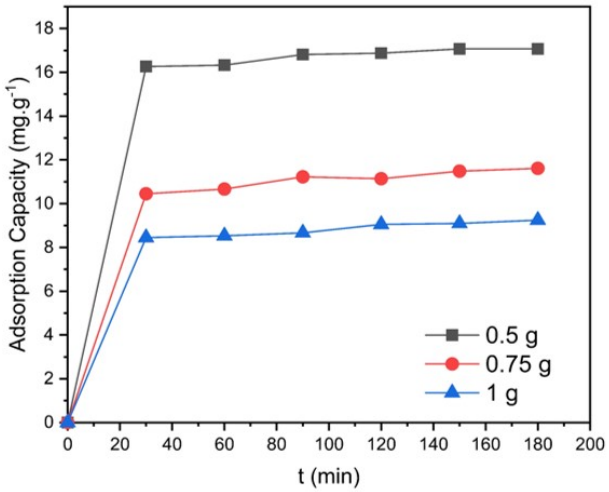

Figure 5. Adsorption Capacity at Different NC Masses

3.2 Batch Adsorption Study

Figure 5 illustrates the effect of adsorbent mass on the adsorption capacity of NC for Fe(III). A reduced NC mass exhibits an enhanced adsorption capacity. The phenomenon can be attributed to the concentration effect at equilibrium, when the adsorbent mass is lower, Fe(III) is inadequately adsorbed onto NC, resulting in a higher Ct value. Consequently, the driving force for the adsorption step remains strong. On the other hand, an increased NC mass facilitates greater Fe(III) removal, leading to a lower Ct value, which subsequently minimizes the driving force and lowers adsorption efficiency. In addition, a higher NC mass may leave some active sites unoccupied because the amount of Fe(III) is insufficient to saturate all available sites, thereby lowering the adsorption capacity. Furthermore, at higher NC masses, particles tend to aggregate, resulting in a diminished effective surface area for the adsorption process, hence reducing

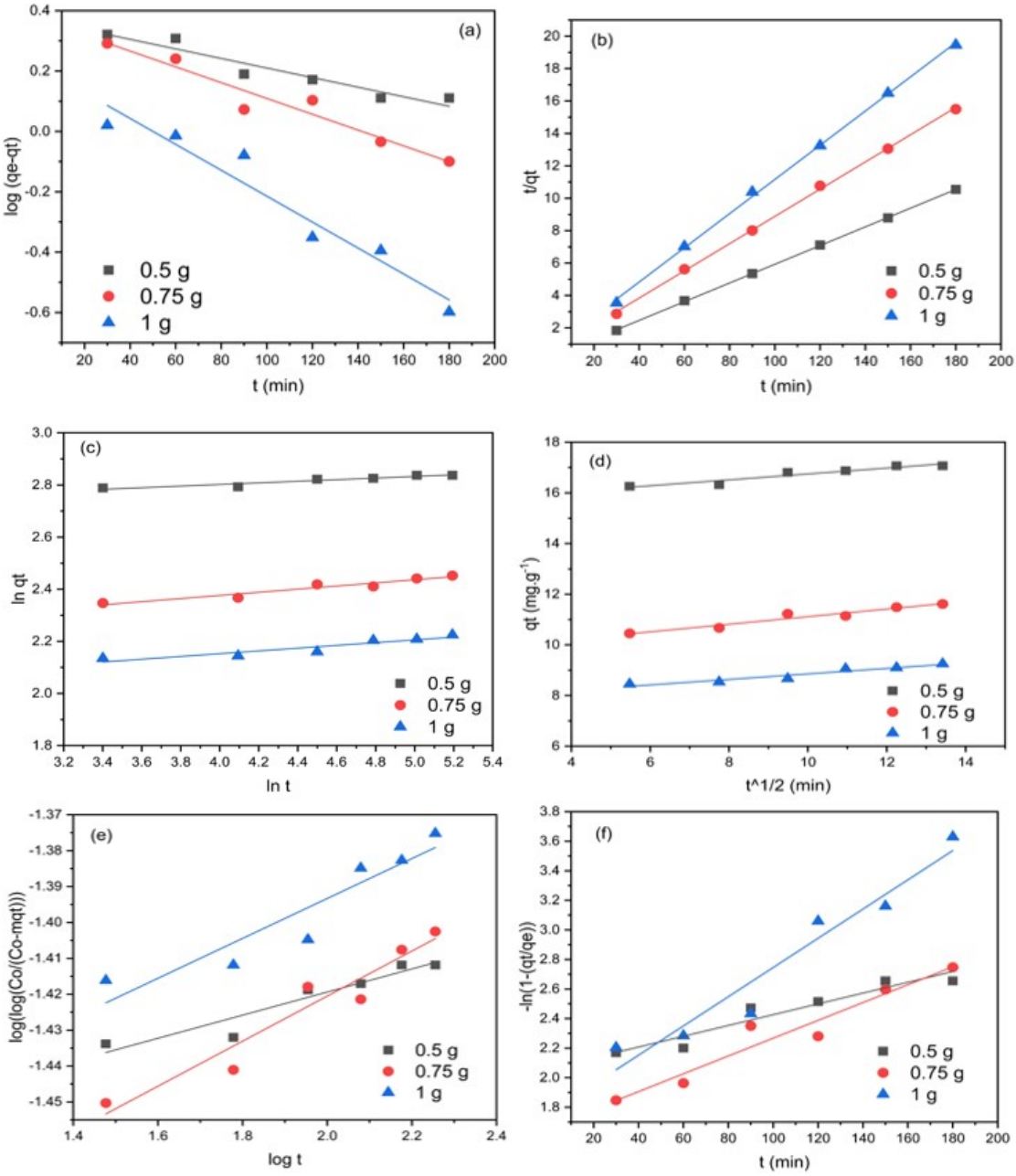

Figure 6. Linear Regression of Several Kinetic Models (a) PFO; (b) PSO; (c) Fractional Power; (d) IPD; (e) Bangham; and (f) LFD

adsorption efficiency.

Moreover, the contact time can significantly influence the adsorption mechanism of Fe(III) by NC. In this study, the contact time ranged from 30 to 180 minutes, as shown in Figure 5. The results indicate that the ability of NC to bind Fe(III) increases with longer contact times, continuing to rise slightly as the system approaches equilibrium. During the first 30 minutes, the adsorption capacity will significantly rise owing to a significant amount of functional sites, facilitating the binding of Fe(III) to the surface of NC and resulting in an elevated adsorption rate. The substantial concentration gradient between Fe(III) and NC promotes mass transfer, hence accelerating the diffusion of Fe(III) to the NC surface, which subsequently decreases with time. Strong physicochemical forces, such as hydrogen bonding, van der Waals forces, and electrostatic attractions, typically contribute to the initial interaction between Fe(III) and NC, supported by the large number of active sites available that make these interactions more favorable.

The adsorption capacity value of NC against Fe(III) in

Table 3. Kinetic Parameters

Kinetic Models	NC Mass (g)		
	0.5	0.75	1
PFO:			
qe ($mg.g^{-1}$)	1.4456	1.4489	1.2395
k_1 (min^{-1})	0.0037	0.0060	0.0069
R^2	0.9146	0.9394	0.9385
PSO:			
qe ($mg.g^{-1}$)	17.3310	11.9048	9.4787
k_2 ($g.mg^{-1}.min^{-1}$)	1881.9800	291.4919	146.2325
R^2	0.9999	0.9993	0.9991
FP:			
a ($mg.g^{-1}.min^2$)	14.5647	8.4638	6.9615
b	0.0308	0.0601	0.0531
R^2	0.9065	0.9290	0.8713
IPD:			
Kint ($mg.g^{-1}.min^{-1/2}$)	0.0314	0.1498	0.1088
C ($mg.g^{-1}$)	0.5858	9.6176	7.7675
R^2	0.9192	0.9288	0.9380
Bangham:			
α	0.0322	0.0628	0.0556
K_B (g)	1.4032	1.0735	0.7596
R^2	0.9065	0.9288	0.8711
LFD:			
k_{fd} (min^{-1})	0.0037	0.0060	0.0099
$t_{1/2}$ (s)	187.2970	115.5000	70.0149
R^2	0.9146	0.9394	0.9385

this study is comparable to or even better to the results of several other types of adsorbents, as evidenced by the numerous past research investigations around the Adsorption of Fe(III) with many different kinds of adsorbents, as shown in Table 2. It implies that NC can be utilized as a reference in the removal of Fe(III). However, additional modifications are required in future research to enhance the adsorption capacity.

3.3 Kinetics Study

Several adsorption kinetic approaches have been applied in examining the potential of NC to removal Fe(III), for example, Pseudo-First-Order (PFO) (Equation 2), Pseudo-Second-Order (PSO) (Equation 3), Fractional Power (FP) (Equation 4), Intra Particle Diffusion (IPD) (Equation 5), Bangham (Equation 6), and Liquid Film Diffusion (LFD) (Equation 7). The kinetic parameters provided in the current experiment can be observed in Table 3. The PFO, PSO, and FP kinetic models explain the kinetic parameters being performed; however, the IPD, Bangham, and LFD kinetic models identify the mechanisms controlling the adsorption process.

The PFO kinetic model (Equation 2) has been widely applied to analyze adsorption rates based on the Lagergren equation, in which the adsorption rate depends on mass diffusion across the wastewater to the adsorbent surface (Alsaiari et al., 2024; Thinojah and Ketheesan, 2022). The parameters of the PFO kinetic model are qe ($mg.g^{-1}$) and k_1 (min^{-1}). The linear regression plot of the PFO kinetic model is derived from the log (qe-qt) versus t values from Equation 2, as shown in Figure 6. The results indicate that the qe value predicted by the PFO model differs significantly from the experimentally obtained qe value, implying that the PFO kinetic model is inappropriate for describing the adsorption of Fe(III) by NC.

The PSO kinetic model (Equation 3) was applied to analyze the adsorption of Fe(III) by NC. The PSO kinetic model assumes that the adsorption process is controlled by chemical interactions or chemisorption, involving the formation of chemical bonds between adsorbate molecules and active sites on the adsorbent surface (Bullen et al., 2021; Tran, 2023). The PSO kinetic model can be evaluated by plotting t/qt vs t from Equation 3, as shown in Figure 6. The results indicated that the PSO kinetic model gives a correlation coefficient ($R^2 > 0.999$). The results suggest that the adsorption of Fe(III) by NC is completely suitable with the PSO kinetic model. Moreover, the qe value derived from the PSO kinetic model exhibits minor disparity when compared to the experimental qe value, so reinforcing the assertion of the model's exceptional suitability. According to the data in Table 3, the qe value will rise simultaneously with an increase in NC mass. Therefore, the parameters derived based on this PSO kinetic model are in accordance with the statement that has been presented earlier in this study. In addition, the influence of NC mass will affect the k_2 value, where there is a decrease in the k_2 value along with the increase in NC mass, as shown in Table 3. This phenomenon can be influenced by active sites, which will be reduced due to particle overlap, the adsorption rate, which will subsequently decrease due to the larger distribution of Fe(III) ions, and the overall control of the diffusion process. The adsorption mechanism of Fe(III) by NC, as described by the PSO kinetic model, may proceed via ion exchange between Fe(III) and the active groups present in NC (such as −OH, −Si−O, and −Al−O) located in clay, as previously elucidated. This occurs as a result of electrostatic interactions between Fe(III) and negatively charged active sites, subsequently leading to the formation of complex compounds through coordinate covalent bonding.

The FP kinetic model (Equation 4) is based on an empirical method applied to analyze adsorption processes that do not follow PFO or PSO accurately. This model is frequently used when the adsorption mechanism is more complex and incorporates more than one rate-controlling component, such

Table 4. Thermodynamic Parameters of Fe(III) Adsorption onto NC

Mass	ΔH°	ΔS°	ΔG° (KJ/mol)		
(g)	(KJ/mol K)	(KJ/mol K)	303 K	313 K	323 K
0.5	10.75	0.040503	-1.5225	-1.92754	-2.33257
0.75	10.16054	0.051417	-5.41884	-5.93301	-6.44718
1	2.038676	0.021809	-4.56954	-4.78763	-5.00572

as external diffusion, intra-particle diffusion, or a combination of physical and chemical adsorption. The FP kinetic model can be evaluated by plotting ln qt vs ln t from Equation 4, as illustrated in Figure 6. Based on the correlation coefficient (R^2) values presented in Table 3, the FP kinetic model tends to produce a lower R^2 value. Therefore, it may be assumed that the adsorption phase of Fe(III) by NC does not adequately fit with the FP kinetic model. The Fe(III) adsorption process typically begins with the migration of Fe(III) ions to the adsorbent surface via a mass diffusion mechanism driven by the concentration gradient. Subsequently, Fe(III) ions are required to traverse the liquid boundary layer during the film diffusion process, which may pose a challenge to the adsorption process if the boundary layer attains sufficient thickness. Moreover, Fe(III) will permeate into the nanoparticle pores during the intraparticle diffusion phase, particularly when the nanoparticle exhibits mesoporous or may manifest as electrostatic bonds, ion exchange with H^+ or Na^+, and the formation of complexes with functional groups such as −OH, −SiO−, or −AlO−. This process may continue until micropores are reached. Upon arrival at the active sites, Fe(III) ions engage in adsorption interactions until equilibrium is established, characterized by the equality of the adsorption and desorption rates.

In the present investigation, the adsorption of Fe(III) by NC was evaluated using the IPD (Equation 5), Bangham (Equation 6), and LFD (Equation 7) kinetic models to elucidate the mechanisms governing the adsorption of Fe(III).

The IPD kinetic model (Equation 5) suggests that the rate of adsorption is governed by the migration of ions into the small pores of the adsorbent, with the key parameter being the value of the intraparticle diffusion constant. This model is typically applied when the adsorption process exhibits a multi-stage pattern and does not pass through the origin, indicating the involvement of other concurrent processes. The parameters of the IPD kinetic model can be estimated by plotting the $t^{1/2}$ vs. q_t values from Equation 5 as illustrated in Figure 6. Based on the data parameters of the IPD kinetic model obtained and given in Table 3, the R^2 value of the IPD kinetic model indicates a tendency value of > 0.9, but is still lower when compared to the PSO kinetic model. This value still exhibits a linear trend, suggesting that intraparticle diffusion contributes to the Fe(III) adsorption by NC, but it does not serve as the primary rate-determining mechanism; instead, it acts as a supporting step during the later stages of adsorption. In addition, the LFD kinetic model (Equation 7) is also applied in the Fe(III) adsorption mechanism via NC, which posits that the transfer of absorbed material ions across the surface of the adsorbent is limited by the act of diffusion barrier in the liquid layer (film). This film layer works as a barrier to prevent the transfer of adsorption material ions of the solution to the adsorbent surface, especially when the ions must pass across the liquid layer boundary created due to the viscosity of the solution or low stirring speed. The LFD Kinetic Model can be produced via graphing the value of $-\ln\left(1-\frac{q_t}{q_e}\right)$ vs. t from Equation 7, which can be seen in Figure 6. The results reveal that the R^2 value of the LFD model is also greater than 0.9, indicating a good linear trend. Therefore, the liquid film diffusion stage also plays a supporting role in the Fe(III) adsorption process by NC.

The data presented in Table 3 further reveal that when the adsorbent mass is lower, the adsorption process tends to be regulated by intraparticle diffusion (IPD) because the number of active sites is limited, allowing Fe(III) ions to diffuse more quickly into the clay pores. Under these conditions, intraparticle diffusion becomes the rate-limiting stage, particularly if the clay structure contains micropores or mesopores. Conversely, with a larger adsorbent mass, the number of active sites on the clay surface increases substantially, resulting in adsorption dominated by the liquid film diffusion process. In this condition, Fe(III) ions must transit through the liquid film layer surrounding the absorbent before they reach its surface, and ion transport across this layer becomes the rate-limiting stage. The variation in mechanism demonstrates that the mass of the adsorbent not only affects the adsorption capacity but also impacts the main kinetic stage, where at smaller amounts the process of diffusion control starts within the pores, while for large amounts the diffusion control is more heavily impacted by the liquid layer surrounding the adsorbent. This is also in agreement with previous investigations undertaken by Bennour (2017), which demonstrates that based on a kinetic model involving an initial rapid adsorption phase due to the abundance of adsorption sites on the clay surface, followed by a slower diffusion-controlled phase when metal ions diffuse into the clay pores. In the LFD kinetic model, the number of the liquid film diffusion rate constant K_{fd} grows with increasing adsorbent mass, and it also has a smaller half-life value $t_{1/2}$,

demonstrating an increase in the efficiency of adsorption kinetics. As the adsorbent mass grows, the number of active sites on the surface increases, thus enhancing the opportunity for Fe(III) ions to be adsorbed. This reduces the diffusion barrier in the liquid layer around the adsorbent, which causes the K_{fd} value to increase. On the other hand, the half-life decreases since adsorption happens faster due to the greater number of active sites available to ensure that Fe(III) ions can directly interact with the adsorbent surface without waiting excessively long. This connection demonstrates that for higher adsorbent masses, the liquid film diffusion mechanism becomes more efficient, maximizing adsorbate transport to the adsorbent surface and accelerating the adsorption phase until a state of equilibrium has been reached.

The Bangham kinetic model (Equation 6) is also applied in analyzing the Fe(III) adsorption mechanism. This model proposes that diffusion in pores (particularly micropores) is the rate-limiting stage of adsorption (Afandy and Sawali, 2024). This model can be derived by plotting the log-log $\left(\frac{C_0}{C_0 - mq_t}\right)$ vs. $\log t$ values from Equation 6, as shown in Figure 5. The parameter findings derived from the Bangham kinetic model, as presented in Table 3, reveal a smaller R^2 value when compared to IPD and LFD models. The smaller coefficient of determination (R^2) value of the Bangham model compared to the IPD and LFD models indicates that the adsorption mechanism is not fully controlled by diffusion through micropores, which is the fundamental presumption of the Bangham model. The Bangham model is normally significant if the adsorption includes ion transport through very small micropores in the adsorbent; however, its small R^2 value shows that this mechanism is not important in the studied system. In contrast, the larger R^2 values of the IPD and LFD models imply that the intraparticle diffusion mechanism into mesopores or macropores (IPD) and ion transport through the liquid film layer around the adsorbent (LFD) contribute more to the adsorption rate. This may be due to the properties of activated clay, which has a bigger pore structure, or the dominance of active sites on the surface that improve the interaction between Fe(III) ions and the adsorbent surface, such that the rate control is more governed by the IPD and LFD mechanisms.

3.4 Thermodynamics Study

Thermodynamic parameters such as ΔS°, ΔH°, and ΔG°, which describe the transfer of dissolved molecules from a fluid to the adsorbent interface, may be shown in Table 4. These parameters can be obtained using linear regression by plotting $\ln K_c$ vs. $1/T$ based on Equation 10. The thermodynamic parameters of Fe(III) adsorption are presented in Table 4.

According to the data in Table 4, the adsorption phase is endothermic (ΔH° positive), suggesting that the adsorption of Fe(III) by NC requires external energy and will be more effective at higher temperatures. The endothermic nature indicates that a temperature rise enhances adsorption capacity, consistent with the Le Chatelier principle, which states that a system will shift in the direction that absorbs heat as temperature increases. The positive ΔH° value (2.0387–10.7500 $\mathrm{kJ\,mol^{-1}\,K^{-1}}$) implies that the adsorption of Fe(III) onto the NC outer layer takes place via physisorption, attributed to the establishment of Van der Waals interactions between Fe(III) and NC. Additionally, adsorption of Fe(III) may occur through electrostatic attraction involving negatively charged sites on NC initiated with H_2SO_4. The light ion exchange activity between Fe(III) and H^+ ions may also occur due to acid residues after the NC activation.

The entropy value (ΔS°) derived from this research showed a positive range of 0.0218 to 0.0405 $\mathrm{kJ\,mol^{-1}\,K^{-1}}$. This suggests an increase in disorder, an increase in degrees of freedom, or a wider energy distribution relative to the state before the adsorption process. This may occur if Fe(III) molecules or ions influence the breakdown of water components from the adsorbent surface, or if a structural transformation of the adsorbent takes place during adsorption. The substitution of Fe(III) ions in solution for more conventional ions via an ion exchange process on the adsorbent surface may enhance the system's regularity. Furthermore, an elevation in entropy may result from the development of a complex between Fe(III) and functional groups on the NC surface, leading to the desorption of water molecules.

The Gibbs free energy value (ΔG°) (Equation 9) obtained in this study indicates that the Fe(III) adsorption process by NC happens spontaneously. Moreover, the ΔG° value suggests that the procedure for adsorption has been generally controlled by the increase in ΔS° rather than alterations in ΔH°. The adsorption appears to be more effective at higher temperatures since the ΔG° values become more negative as temperature increases.

4. CONCLUSIONS

This work has demonstrated that the modification of natural clay with sulfuric acid significantly enhanced both the chemical and physical characteristics of the material, consequently augmenting its adsorption capacity for Fe(III). The kinetic study findings verified the conclusions that the pseudo-second-order (PSO) model most effectively matched the experimental result, indicating that the adsorption process proceeded via a chemisorption mechanism. Thermodynamic analysis produced a negative ΔG° value, confirming that the adsorption phase occurred spontaneously, and a positive ΔH° value, indicating endothermic properties; thus, increasing temperatures accelerated the adsorption process. The modified clay from Morowali presents a promising opportunity as a cost-effective, efficient, and environmentally friendly adsorbent for treating wastewater containing Fe(III), particularly in the nickel sector. These findings provide a solid framework for leveraging local resources in sustainable

pollution management techniques.

5. ACKNOWLEDGEMENT

The author is pleased to provide his deepest gratitude to the Politeknik Industri Logam Morowali for giving support and assistance in carrying out this research.

REFERENCES

Abbaspour, N., R. Hurrell, and R. Kelishadi (2014). Review on Iron and Its Importance for Human Health. *Journal of Research in Medical Sciences*, **19**(2); 3–11

Abdel-Ghafar, H. M., E. A. Abdel-Aal, and B. E. El Anadouli (2020). Iron Removal from Ground Water Using Egyptian Cost-Effective Clay Minerals. *Applied Chemical Engineering*, **3**(1); 23–30

Adawiyah, R., N. Yuliasari, Y. Hanifah, K. Alawiyah, and N. R. Palapa (2021). Utilizing *Areca catechu* L. Fruit Peel-Derived Biochar and Hydrochar for. *Indonesian Journal of Environmental Management and Sustainability*, **8**(4); 135–144

Afandy, M. A. and F. D. I. Sawali (2024). Effect of Concentration on Kinetics and Thermodynamics Parameter in the Cu(II) Removal by Activated Zeolite. *Jurnal Integrasi Proses*, **13**(2); 174–183

Al-Odayni, A. B., F. S. Alsubaie, N. A. Y. Abdu, H. M. Al-Kahtani, and W. S. Saeed (2023). Adsorption Kinetics of Methyl Orange from Model Polluted Water onto N-Doped Activated Carbons Prepared from N-Containing Polymers. *Polymers*, **15**(9); 1983

Alsaiari, R., I. Shedaiwa, F. A. Al-Qadri, E. M. Musa, H. Alqahtani, F. Alkorbi, N. A. Alsaiari, and M. M. Mohamed (2024). *Peganum Harmala* L. Plant as Green Non-Toxic Adsorbent for Iron Removal from Water. *Archives of Environmental Protection*, **50**(1); 3–12

Auta, M. and B. H. Hameed (2013). Acid Modified Local Clay Beads as Effective Low-Cost Adsorbent for Dynamic Adsorption of Methylene Blue. *Journal of Industrial and Engineering Chemistry*, **19**(4); 1153–1161

Bahabadi, F. N., M. H. Farpoor, and M. H. Mehrizi (2016). Removal of Cd, Cu and Zn Ions from Aqueous Solutions Using Natural and Fe Modified Sepiolite, Zeolite and Palygorskite Clay Minerals. *Water Science and Technology*, **75**(2); 340–349

Bakalár, T., M. Kaňuchová, A. Girová, H. Pavolová, R. Hromada, and Z. Hajduová (2020). Characterization of Fe(III) Adsorption Onto Zeolite and Bentonite. *International Journal of Environmental Research and Public Health*, **17**(16); 1–13

Benjelloun, M., Y. Miyah, G. Akdemir Evrendilek, F. Zerrouq, and S. Lairini (2021). Recent Advances in Adsorption Kinetic Models: Their Application to Dye Types. *Arabian Journal of Chemistry*, **14**(4); 103031

Bennour, H. A. M. (2017). Effect of Acid Activation on Adsorption of Iron and Manganese Using Libyan Bentonite Clay. *Chemical Science Transactions*, **6**(2); 209–218

Billah, R. E. K., Y. Haddaji, O. Goudali, M. Agunaou, and A. Soufiane (2021). Removal and Regeneration of Iron (III) from Water Using New Treated Fluorapatite Extracted from Natural Phosphate as Adsorbent. *Biointerface Research in Applied Chemistry*, **11**(5); 13130–13140

Bullen, J. C., S. Saleesongsom, K. Gallagher, and D. J. Weiss (2021). A Revised Pseudo-Second-Order Kinetic Model for Adsorption, Sensitive to Changes in Adsorbate and Adsorbent Concentrations. *Langmuir*, **37**(10); 3189–3201

Caccamo, M. T., G. Mavilia, L. Mavilia, D. Lombardo, and S. Magazù (2020). Self-Assembly Processes in Hydrated Montmorillonite by FTIR Investigations. *Materials*, **13**(5); 1100

Costea, I. F., A.-M. Ceoromila, A. Tabacaru, and G. Carac (2024). Investigation of Chitosan Flakes in the Adsorption of Fe(III) Ions from Acidic Solution. *Revista de Chimie*, **75**(2); 1–10

Das, D. and B. K. Nandi (2019). Removal of Fe(II) Ions from Drinking Water Using Electrocoagulation (EC) Process: Parametric Optimization and Kinetic Study. *Journal of Environmental Chemical Engineering*, **7**(3); 103116

Elewa, A. M., A. A. Amer, M. F. Attallah, H. A. Gad, Z. A. M. Al-Ahmed, and I. A. Ahmed (2023). Chemically Activated Carbon Based on Biomass for Adsorption of Fe(III) and Mn(II) Ions from Aqueous Solution. *Materials*, **16**(3); 1251

Enaime, G., A. Baçaoui, A. Yaacoubi, and M. Lübken (2020). Biochar for Wastewater Treatment—Conversion Technologies and Applications. *Applied Sciences*, **10**(10); 3492

Guo, X., A. Liu, J. Lu, X. Niu, M. Jiang, Y. Ma, X. Liu, and M. Li (2020). Adsorption Mechanism of Hexavalent Chromium on Biochar: Kinetic, Thermodynamic, and Characterization Studies. *ACS Omega*, **5**(42); 27323–27331

Herrera, K., L. F. Morales, N. A. Tarazona, R. Aguado, and J. F. Saldarriaga (2022). Use of Biochar from Rice Husk Pyrolysis: Part A: Recovery as an Adsorbent in the Removal of Emerging Compounds. *ACS Omega*, **7**(9); 7625–7637

Inyinbor, A. A., F. A. Adekola, and G. A. Olatunji (2016). Kinetics, Isotherms and Thermodynamic Modeling of Liquid Phase Adsorption of Rhodamine B Dye Onto *Raphia hookerie* Fruit Epicarp. *Water Resources and Industry*, **15**; 14–27

Islam, M. Z. and M. G. Mostafa (2024). Iron, Manganese, and Lead Contamination in Groundwater of Bangladesh: A Review. *Water Practice and Technology*, **19**(3); 745–760

Kalabegashvili, N., G. Balarjishvili, D. Ioseliani, L. Samkharadze, N. Nonikashvili, and I. Mikadze (2022). Iron (III) Adsorption on Perlite. *World Journal of Advanced Research and Reviews*, **15**(1); 644–650

Khatri, N., S. Tyagi, and D. Rawtani (2017). Recent Strategies for the Removal of Iron from Water: A Review.

Journal of Water Process Engineering, **19**(13); 291–304

Kulkarni, S. J. (2016). A Review on Studies and Research on Iron Removal. *International Journal of Science and Healthcare Research*, **1**(2); 49

Kumar, R., P. Sharma, P. K. Sharma, P. K. Rose, R. K. Singh, N. Kumar, P. K. Sahoo, J. P. Maity, A. Ghosh, M. Kumar, P. Bhattacharya, and A. Pandey (2023). Rice Husk Biochar - A Novel Engineered Bio-Based Material for Transforming Groundwater-Mediated Fluoride Cycling in Natural Environments. *Journal of Environmental Management*, **343**; 118222

Langeroodi, N. S., Z. Farhadravesh, and A. D. Khalaji (2018). Optimization of Adsorption Parameters for Fe(III) Ions Removal from Aqueous Solutions by Transition Metal Oxide Nanocomposite. *Green Chemistry Letters and Reviews*, **11**(4); 404–413

Latunde-Dada, G. O. (2024). Iron Intake and Human Health. *Nutrients*, **16**(2); 206

Li, Z., Z. Zheng, H. Li, D. Xu, X. Li, and L. Xiang (2023). Review on Rice Husk Biochar as an Adsorbent for Soil and. *Plants*, **12**(1524); 1–19

Menkiti, M., I. Ezemagu, and S. Singaraju (2018). Focus on Adsorptive Equilibrium, Kinetics and Thermodynamic Components of Petroleum Produced Water Biocoagulation Using Novel *Tympanotonos Fuscatus* Extract. *Petroleum*, **4**(1); 56–64

Middea, A., L. d. S. Spinelli, F. G. de Souza Junior, T. d. L. A. P. Fernandes, L. C. de Lima, V. M. T. S. Barthem, O. d. F. M. Gomes, and R. Neumann (2024). Removal of Fe_3^+ Ions from Aqueous Solutions by Adsorption on Natural Eco-Friendly Brazilian Palygorskites. *Mining*, **4**(1); 37–57

Mopoung, S., P. Moonsri, W. Palas, and S. Khumpai (2015). Characterization and Properties of Activated Carbon Prepared from Tamarind Seeds by KOH Activation for Fe(III) Adsorption from Aqueous Solution. *Scientific World Journal*, **2015**(1); 415961

Nahiun, K., B. Sarker, K. N. Keya, F. I. Mahir, S. Shahida, and R. A. Khan (2021). A Review on the Methods of Industrial Waste Water Treatment. *Scientific Review*, **73**; 20–31

Ngkoimani, L. O. and M. Chaerul (2017). Impacts of Nickel Laterite Post-Mining Activities on the Level of Heavy Metal Contamination in River Sediments. *Advances in Social Science, Education and Humanities Research (ASSEHR)*, **149**(Icest); 240–242

Oladimeji, T. E., M. Oyedemi, M. E. Emetere, O. Agboola, J. B. Adeoye, and O. A. Odunlami (2024). Review on the Impact of Heavy Metals from Industrial Wastewater Effluent and Removal Technologies. *Heliyon*, **10**(23); e40370

Osmić, S., A. Odobašić, and S. Begić (2024). The Influence of Acid Activation on Surface Characteristics of Natural Bentonite. *International Research Journal of Pure and Applied Chemistry*, **25**(5); 35–42

Pakade, V. E., N. T. Tavengwa, and L. M. Madikizela (2019). Recent Advances in Hexavalent Chromium Removal from Aqueous Solutions by Adsorptive Methods. *RSC Advances*, **9**(45); 26142–26164

Palapa, N. R., A. Amri, and Y. Hanifah (2023). Potential Indonesian Rice Husk for Wastewater Treatment Agricultural Waste Preparation and Dye Removal Application. *Indonesian Journal of Environmental Management and Sustainability*, **7**(4); 160–165

Purnamasari, I. and E. Supraptiah (2017). Adsorption Kinetics of Fe and Mn with Using Fly Ash from PT Semen Baturaja in Acid Mine Drainage. *Indonesian Journal of Environmental Management and Sustainability*, **1**(1); 17–20

Raji, Z., A. Karim, A. Karam, and S. Khalloufi (2023). Adsorption of Heavy Metals: Mechanisms, Kinetics, and Applications of Various Adsorbents in Wastewater Remediation—A Review. *Waste*, **1**(3); 775–805

Rosa, M. S. L., T. Knoerzer, F. C. Figueiredo, and J. R. dos Santos Júnior (2020). Clarification of Used Lubricating Oils by Application of Chemically-Modified Clays. *Ceramica*, **66**(378); 130–136

Salam, M. A., R. M. El-Shishtawy, and A. Y. Obaid (2014). Synthesis of Magnetic Multi-Walled Carbon Nanotubes/Magnetite/Chitin Magnetic Nanocomposite for the Removal of Rose Bengal from Real and Model Solution. *Journal of Industrial and Engineering Chemistry*, **20**(5); 3559–3567

Satchawan, S., P. Phuengphai, A. Ratanamanee, and N. Meethong (2022). Kinetic and Equilibrium Studies of Fe(III) Sorption from an Aqueous Solution Using Palmyra Palm Fruit Fibres as a Biosorbent. *Applied Sciences*, **12**(20)

Sirotiak, M., B. Alica, and L. Blinová (2014). Uv-Vis Spectrophotometric Determinations of Selected Elements in Modelled Aqueous Solutions. *Journal of Environmental Protection, Safety, Education and Management*, **2**(3); 75–87

Song, P. N., J. G. Mahy, C. Calberg, A. Farcy, J. Caucheteux, N. Fagel, and S. D. Lambert (2023). Influence of Thermal and Acidic Treatments on the Morphology of a Natural Kaolinitic Clay Mineral. *Results in Surfaces and Interfaces*, **12**(July); 100131

Thinojah, T. and B. Ketheesan (2022). Iron Removal from Groundwater Using Granular Activated Carbon Filters by Oxidation Coupled with the Adsorption Process. *Journal of Water and Climate Change*, **13**(5); 1985–1994

Tran, H. N. (2023). Applying Linear Forms of Pseudo-Second-Order Kinetic Model for Feasibly Identifying Errors in the Initial Periods of Time-Dependent Adsorption Datasets. *Water (Switzerland)*, **15**(6); 1231

Wang, B., J. Lan, C. Bo, B. Gong, and J. Ou (2023). Adsorption of Heavy Metal Onto Biomass-Derived Activated Carbon: Review. *RSC Advances*, **13**(7); 4275–4302

Wang, P., X. Shen, S. Qiu, L. Zhang, Y. Ma, and J. Liang

(2024). Clay-Based Materials for Heavy Metals Adsorption: Mechanisms, Advancements, and Future Prospects in Environmental Remediation. *Crystals*, **14**(12); 1046

Xie, S., L. Huang, C. Su, J. Yan, Z. Chen, M. Li, M. Du, and H. Zhang (2024). Application of Clay Minerals as Adsorbents for Removing Heavy Metals from the Environment. *Green and Smart Mining Engineering*, **1**(3); 249–261

Yang, J., B. Huang, and M. Lin (2020). Adsorption of Hexavalent Chromium from Aqueous Solution by a Chitosan/Bentonite Composite: Isotherm, Kinetics, and Thermodynamics Studies. *Journal of Chemical and Engineering Data*, **65**(5); 2751–2763

Zein, R., Y. Prestica, D. Deswati, and P. Ramadhani (2023). Utilization of Coffee Peel Waste as Biosorbent for Rhodamine B Dye. *Indonesian Journal of Environmental Management and Sustainability*, **9**(1); 36–45

Šuránek, M., Z. Melichová, M. M. Mirković, M. Ivanović, V. B. Pavlović, L. Kljajević, and S. Nenadović (2023). The Study of Cu(II) Adsorption Onto Synthetically Modified Geopolymers. *Sustainability (Switzerland)*, **15**(4); 2869

